Precision Measurement of the Longitudinal Double-spin Asymmetry for Inclusive Jet Production in Polarized Proton Collisions at $\sqrt{s} = 200$ GeV/c

(The STAR Collaboration)

We report a new high-precision measurement of the inclusive jet longitudinal double-spin asymmetry, A_{LL}, in polarized pp collisions at center-of-mass energy $\sqrt{s} = 200$ GeV. The STAR data place stringent constraints on modern polarized parton densities extracted from next-to-leading order global analyses of deep inelastic scattering (DIS), semi-inclusive DIS, and RHIC pp data. These results provide the first experimental indication of non-zero gluon polarization in the Bjorken-x region sampled at RHIC.

A fundamental and long standing puzzle in Quantum Chromodynamics (QCD) concerns how the intrinsic spin and orbital angular momentum of the gluons, valence and sea quarks sum to give the proton spin of $\hbar/2$. The flavor summed quark and anti-quark spin contribution ($\Delta\Sigma$) is the only distribution that has been measured to a relative precision of ∼10%, and it accounts for less than a third of the total proton spin budget [1–5]. Due to the limited kinematic reach of fixed target experiments, the same polarized deep-inelastic scattering (DIS) data [6] used to extract $\Delta\Sigma$ are capable of only loosely constraining the gluon spin (ΔG) contribution.

The measurement of asymmetries directly sensitive to the gluon helicity distribution was a primary motivation for establishing the spin structure program at the Relativisitic Heavy Ion Collider (RHIC). Since the commencement of the RHIC spin program, several inclusive jet [7–9] and pion [10–13] asymmetry measurements have been incorporated into the next-to-leading-order (NLO) perturbative QCD (pQCD) fits. While these data provide significant constraints on ΔG by ruling out large positive or negative contributions to the proton spin, they lack the statistical power to distinguish even a moderate gluon contribution, comparable to the quark contribution, from zero. The inclusive jet asymmetries presented here benefit from a significant increase in the event sample as well as improved jet reconstruction and correction techniques, allowing for the first time a measurement capable of discerning a non-zero ΔG.

The inclusive jet longitudinal double-spin asymmetry, A_{LL}, is defined as:

$$A_{LL} = \frac{\sigma^{++} - \sigma^{+-}}{\sigma^{++} + \sigma^{+-}}, \qquad (1)$$

where $\sigma^{++}(\sigma^{+-})$ is the differential cross section when the beam protons have the same (opposite) helicities. This asymmetry provides direct sensitivity to the gluon polarization [14] because inclusive jet production in $\sqrt{s} = 200$ GeV/c collisions is dominated by quark-gluon (qg) and gluon-gluon (gg) scattering for the jet transverse momenta ($5 < p_T < 35$ GeV/c) discussed in this analysis.

The data presented here are extracted from an integrated luminosity of $20\,\mathrm{pb}^{-1}$ recorded in the year 2009 with the STAR detector [15] at RHIC. The polarization was measured independently for each of the two counter-rotating proton beams (hereafter designated blue (B) and yellow (Y)) and for each fill using Coulomb-Nuclear Interference (CNI) proton-carbon polarimeters [16], which were calibrated via a polarized atomic hydrogen gas-jet target [17]. Averaged over RHIC fills, the luminosity-weighted polarizations for the two beams were $P_B = 0.574$ and $P_Y = 0.573$, with a 6.5% relative uncertainty on the product $P_B P_Y$. The helicity patterns of the colliding beam bunches were changed between beam fills to minimize systematic uncertainties in the A_{LL} measurement. Segmented Beam-Beam Counters (BBC) [18] located up and downstream of the STAR interaction region ($3.3 < |\eta| < 5$) measured the helicity-dependent relative luminosities and served as local polarimeters.

The STAR subsystems used to measure jets are the Time Projection Chamber (TPC) and the Barrel (BEMC) and Endcap (EEMC) Electromagnetic Calorimeters [15]. The TPC provides tracking for charged particles in the 0.5 T solenoidal magnetic field for pseudo-rapidities $|\eta| < 1.3$ and 2π in the azimuthal angle ϕ. The BEMC and EEMC cover a fiducial area of $-1 < \eta < 2$ and $0 < \phi < 2\pi$, and provided triggering and detection of photons and electrons.

Events were recorded if they satisfied the jet patch (JP) trigger condition in the BEMC or EEMC. The JP trigger required a $\Delta\eta \times \Delta\phi = 1 \times 1$ patch of towers to exceed a transverse energy threshold of 5.4 (JP1, prescaled) or 7.3 (JP2) GeV, or two adjacent patches to each exceed 3.5 GeV (AJP). The implementation of the AJP condition combined with a reconfiguration of the jet patches so that they overlapped in η resulted in a 37% increase in jet acceptance compared to previous years [7, 8]. Upgrades in the data acquisition system allowed STAR to record events at several hundred Hz and ∼5% dead time compared with 40 Hz and 40% dead time during the 2006 run [7].

Jets were reconstructed using the mid-point cone algorithm [19] with a radius of 0.7 and the anti-k_T algorithm [20], as implemented in the FastJet package [21], for radius parameters ranging from 0.5-0.7. Both algorithms used TPC tracks and calorimeter towers as input for clustering. The jet asymmetries presented in this Letter utilize the anti-k_T algorithm with a radius parameter $R = 0.6$. The change from the mid-point cone algorithm used in previous STAR inclusive jet analyses

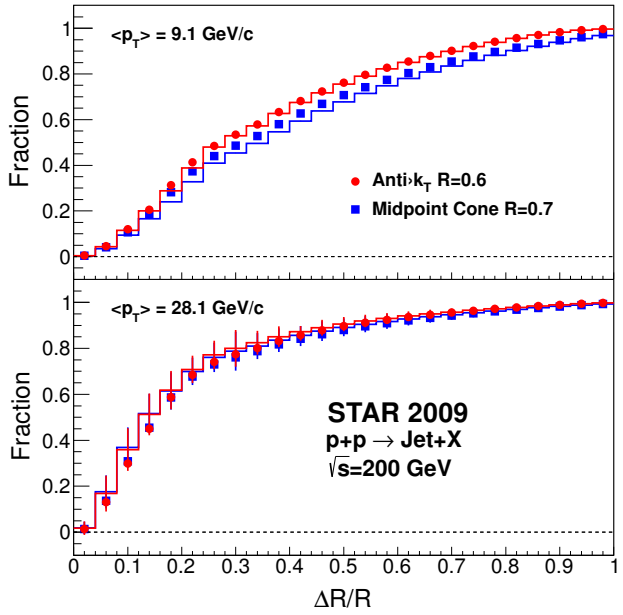

FIG. 1: (Color online.) Fraction of the total jet transverse energy E_T contained in a cone of radius ΔR centered around the jet thrust axis. The E_T fraction is plotted as a function of the ratio $\Delta R/R$ for two different jet definitions for both data (points) and simulations (histograms). The error bars show the simulation statistics. Those for the data are smaller than the points.

[7–9] was motivated by studies indicating that anti-k_T jets are less susceptible to pile-up and underlying event contributions. The difference between the two jet algorithms is illustrated in the jet profiles at low and high jet p_T shown in Fig. 1. At low-p_T, pile-up and underlying event can provide a relatively significant contribution to the jet energy. These contributions distort the relation between the jet energy and that of the parent hard-scattered parton. They also preferentially add energy to the jet periphery, which can introduce trigger bias. The upper panel of Fig. 1 shows that the anti-k_T algorithm integrates a larger fraction of the jet energy at a given distance from the jet thrust axis than the mid-point cone algorithm. The core of jets reconstructed with the anti-k_T algorithm is harder, and those jets are less affected by soft particles. At high-p_T, where the presence of soft particles from pile-up and underlying event is less important, both jet algorithms perform similarly, as shown in the lower panel of Fig. 1. In all cases, we obtain good agreement between data and simulations. $R = 0.6$ was chosen to minimize jet energy scale corrections. A comparison of the fully corrected mid-point cone and anti-k_T inclusive jet A_{LL} values showed no statistically significant difference.

Jets were required to have $p_T > 5$ GeV/c and $|\eta| < 1.0$ in order to minimize the effects of the detector acceptance on the jet energy scale. Beam backgrounds from upstream sources, observed as neutral energy deposits in the B/EEMC, were minimized by requiring the neutral energy fraction (NEF) of the jet energy to be less than 0.94. Only jets which pointed to a triggered jet patch (or pair of patches for the AJP trigger) were considered for analysis. The top panel in Fig. 2 demonstrates the effect of the calorimeter trigger on the jet NEF. The higher threshold JP2 trigger skews the sample to larger neutral energies, especially for lower p_T jets reconstructed near the trigger threshold. The lower panel shows how these biases decrease with increasing jet p_T.

Most frequently charged hadrons deposit energy equivalent to a minimum ionizing particle (MIP) in the calorimeter towers. Since the TPC reconstructs the momentum of all charged particles, the inclusion of tower energy from charged hadrons results in an overestimation of the jet energy. Fluctuations in the deposited tower energy when charged hadrons shower further distort the jet energy and degrade the jet energy resolution. In previous STAR jet analyses [7–9], this hadronic energy was removed from the jet by subtracting a MIP from any BEMC or EEMC tower with a charged track passing through it. In this analysis, up to the total p_T of the charged track was subtracted from the E_T of the matched tower. This procedure reduces the jet energy scale corrections and results in an improved jet energy

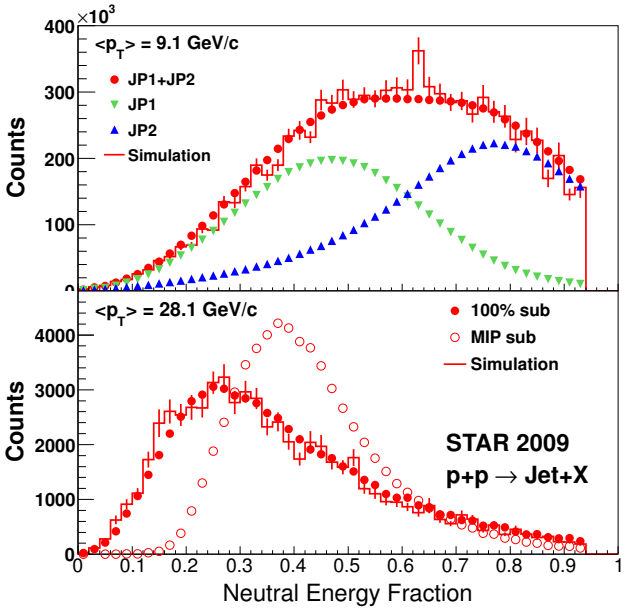

FIG. 2: (Color online.) Jet neutral energy fraction (NEF) comparing data (points) with simulations (histograms). The broad flat distribution in the upper panel arises from nearly equal contributions from the two different trigger thresholds. The lower panel illustrates the impact on NEF of the different hadronic correction schemes discussed in the text. The error bars show the simulation statistics. Those for the data are smaller than the points.

resolution, ∼18% compared to ∼23% in previous analyses. The bottom panel of Fig. 2 demonstrates the effect of this new hadronic subtraction scheme on the jet NEF.

Simulated events are used to calculate jet energy scale corrections and to estimate systematic ~~errors~~. This analysis utilized a simulation sample constructed from QCD events generated using the Perugia 0 tune in PYTHIA 6.425 [22]. The PYTHIA events were processed through the STAR detector response package, which is based on GEANT 3 [23], and then embedded into the detector response from randomly triggered data events. The TPC tracks and calorimeter hits reconstructed from the embedded simulation sample incorporate the same beam backgrounds and pile-up contributions as the data sample, resulting in the excellent agreement between the data and simulation distributions shown in Figs. 1 and 2.

The jet p_T reconstructed at the *detector* level was corrected to both the *particle* and *parton* level. Particle jets have been corrected for trigger and detector efficiency and resolution effects, while parton jets include additional corrections for hadronization and underlying event effects. The anti-k_T algorithm with $R = 0.6$ was used to reconstruct particle and parton jets from the PYTHIA record for events in the simulation sample described above. Detector level jets were matched to the particle (parton) jet closest in $\eta - \phi$ space and within a $\Delta R \leq 0.5$. Association probabilities ranged from 99% in the lowest p_T bin to 100% for $p_T > 9.9$ GeV/c for particle jets and from 76% in the lowest p_T bin and 86% in the next bin to > 98% for $p_T > 9.9$ GeV/c for parton jets. Asymmetry values are then plotted at ~~the~~ the average particle (parton) jet p_T for each detector jet p_T bin. The average particle and parton jet p_T's and associated ~~errors~~ are given in online tables located on the STAR publication webpage.

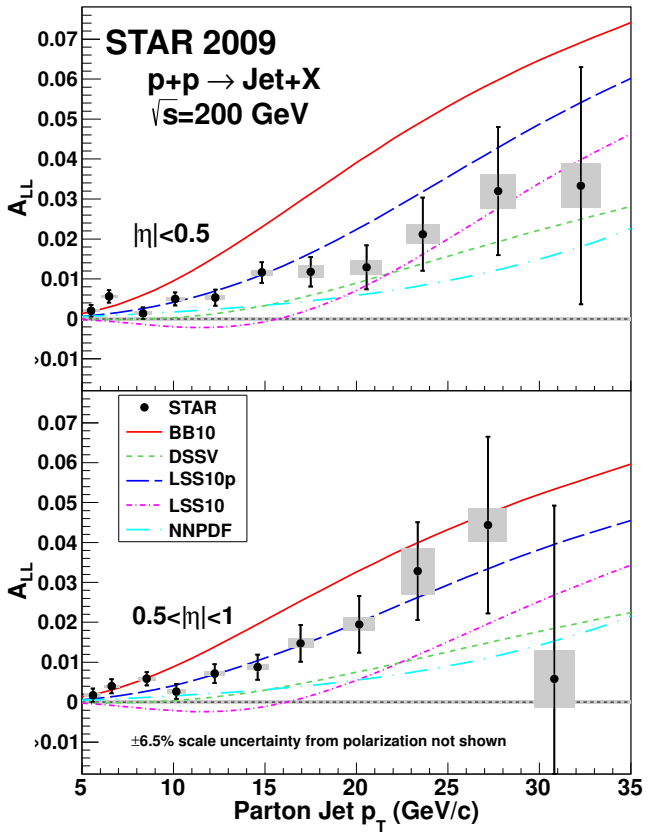

FIG. 3: (Color online.) Midrapidity ($|\eta| < 0.5$, upper panel) and forward rapidity ($0.5 < |\eta| < 1$, lower panel) inclusive jet A_{LL} vs parton jet p_T, compared to predictions from several NLO global analyses. The error bars are statistical. The gray boxes show systematic uncertainties.

The asymmetry A_{LL} was evaluated according to,

$$A_{LL} = \frac{\sum (P_B P_Y)\,(N^{++} - R N^{+-})}{\sum (P_B P_Y)^2\,(N^{++} + R N^{+-})}, \qquad (2)$$

in which $P_{B,Y}$ are the measured beam polarizations, N^{++} and N^{+-} denote the inclusive jet yields for equal and opposite proton beam helicity configurations, and R is the measured relative luminosity. Each sum is over 10 to 60 minute long runs, a period much shorter than typical time variations in critical quantities such as $P_{B,Y}$ and R. Typical values of R range from 0.85 to 1.2 depending on fill and bunch pattern.

Figure 3 shows the inclusive jet A_{LL} plotted as a function of parton jet p_T for two η bins. The STAR trigger biases the data sample by altering the natural subprocess fractions (gg vs. qg vs. qq) predicted by NLO pQCD calculations. Similarly, detector and trigger resolutions may smear and distort the raw A_{LL} values. The size of these effects depends on the value and shape of the gluon distribution as a function of the lightcone momentum fraction x. The raw A_{LL} values were corrected for trigger and reconstruction bias effects by using the simulation to compare asymmetries at the detector, particle and parton levels. PYTHIA is not a polarized generator, but asymmetries can be constructed by using the kinematics of the hard interaction to access polarized and unpolarized parton distribution functions (PDFs) and calculate the partonic scattering cross-sections on an event by event basis. In this way the A_{LL} for three sets of polarized PDFs - DSSV [1, 2], DSSV09a, and LSS10p [4] - were compared. DSSV09a is a private version of the DSSV codes that incorporates the data presented in this Letter. The average of the minimum and maximum $\delta A_{LL} = A_{LL}^{detector} - A_{LL}^{particle(parton)}$ values for each particle and parton jet p_T were used to correct the raw A_{LL} by amounts ranging from 0.0002 at low p_T to 0.0011 at high p_T.

The heights of the shaded ~~error boxes~~ on the A_{LL} points in Fig. 3 reflect the quadrature sum of the systematic uncertainties due to corrections for the trigger and reconstruction bias ($2 - 55 \times 10^{-4}$) and residual transverse polarization ($3 - 26 \times 10^{-4}$), both of which are pri-

marily point-to-point. Contributions to A_{LL} from non-collision backgrounds, such as cosmic rays and beam-gas interactions, were estimated to be less than 2% of the statistical uncertainty on A_{LL} for all jet p_T bins and deemed negligible. The relative luminosity uncertainty ($\pm 5 \times 10^{-4}$), which is common to all the points, is shown by the gray band on the horizontal axis. The width of the shaded error boxes reflects the total systematic error on the jet energy scale. This includes calorimeter tower gain and efficiency and TPC tracking efficiency and momentum resolution effects. An additional uncertainty to account for discrepancies between the NLO and PYTHIA cross-sections was added in quadrature when correcting back to the parton jet level. At the parton level the PYTHIA-NLO shift uncertainty dominates for most bins, making the final energy scale uncertainties highly correlated. Longitudinal single-spin asymmetries, A_L, measure parity-violating effects arising from weak interactions and are expected to be negligible relative to the 2009 statistical errors. A_L was measured and found to be consistent with zero for each beam.

The theoretical curves in Fig. 3 illustrate the expected A_{LL} if the polarized PDF associated with the corresponding global analysis is used as input. These predictions were made by inserting the polarized PDFs from BB [3], DSSV [1, 2], LSS [4] and NNPDF [5] into the NLO jet production code of Mukherjee and Vogelsang [24]. The BB10 and NNPDF polarized PDFs fit only inclusive DIS data, while LSS fits both inclusive and semi-inclusive DIS (SIDIS) datasets. LSS provides two distinct solutions for the polarized gluon density of nearly equal quality. The LSS10 gluon density has a node at $x \sim 0.2$, and the LSS10p gluon is positive definite at the input scale $Q_0^2 = 2.5$ GeV^2. DSSV is the only fit that incorporates DIS, SIDIS, and RHIC pp data.

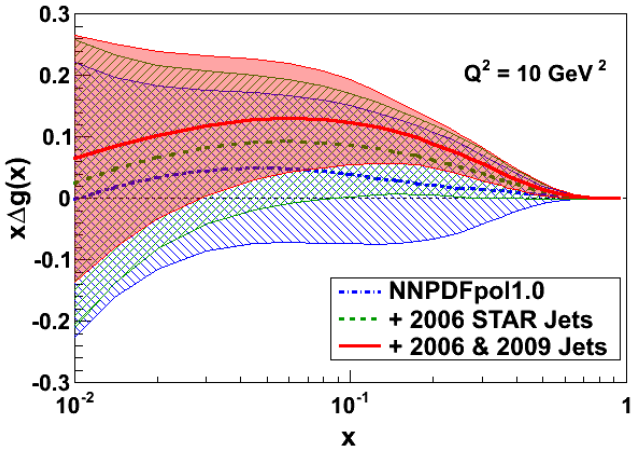

FIG. 4: (Color online.) Gluon polarizations from NNPDF (blue dot-dashed curve, 135^0 hatched uncertainty band) [5], and from modified versions of NNPDF that we obtain when including the 2006 (green dashed curve, 45^0 hatched uncertainty band) or 2006+2009 (red solid curve and uncertainty band) STAR inclusive jet A_{LL} results through reweighting.

The STAR jet data fall between the predictions of BB10 and DSSV. In both cases, the measurements fall within the quoted uncertainty bands. LSS10p is consistent with the STAR jet data ($\chi^2 = 22.5$ for 22 degrees of freedom). In contrast, the STAR jet asymmetries are systematically above the predictions of LSS10 and fall outside the LSS10 uncertainty band for $p_T < 15$ GeV/c. The STAR jet asymmetries are also systematically above the predictions of NNPDF. At forward rapidity for $p_T > 17$ GeV/c, they fall outside the NNPDF uncertainty band.

The NNPDF group has developed a reweighting method to include new experimental data into an existing PDF set without the need to repeat the entire fitting process [25, 26]. We have implemented this method to produce modified NNPDF fits that include the 2006 STAR jet data [7] and the 2006+2009 STAR jet data. We find that the jet data have a negligible impact on the polarized quark and anti-quark distributions, but a significant impact on the polarized gluon distribution. Figure 4 shows the original NNPDF polarized gluon distribution as a function of x at $Q^2 = 10$ GeV^2, as well as the modified fits with the 2006 and 2006+2009 STAR data. The integral of $\Delta g(x)$ over the range $0.05 < x < 0.5$ is 0.06 ± 0.18 for the original NNPDF fit and 0.21 ± 0.10 when the fit is reweighted using the STAR jet data. The inclusion of the STAR jet data results in a substantial reduction in the uncertainty of $x\Delta g(x)$ and indicates a preference for the gluon helicity contribution to be positive in the RHIC kinematic range.

Plan to add paragraph here about new DSSV fit including '09 RHIC data from companion article.

In summary, we report a new high-precision measurement of the inclusive jet longitudinal double-spin asymmetry A_{LL} in polarized pp collisions at $\sqrt{s} = 200$ GeV. The STAR data fall between the predictions of DSSV and BB10. LSS10p (positive solution) is consistent with our data within uncertainties, whereas LSS10 (node solution) is excluded. Inclusion of these data into NNPDF via reweighting shows they provide the first experimental indication of non-zero gluon polarization in the range $0.05 < x < 0.5$ sampled at RHIC. A new global analysis that includes the STAR jet data presented here is needed to extract a more precise polarized gluon density and its error estimate.

We would like to thank (insert appropriate contacts for our theory friends from DSSV, BB, LSS and NNPDF here) for information regarding their respective polarized PDF sets. We thank the RHIC Operations Group and RCF at BNL, the NERSC Center at LBNL, the KISTI Center in Korea and the Open Science Grid consortium for providing resources and support. This work was supported in part by the Offices of NP and HEP within the U.S. DOE Office of Science, the U.S. NSF, CNRS/IN2P3, FAPESP CNPq of Brazil, Ministry of Ed. and Sci. of the

Russian Federation, NNSFC, CAS, MoST and MoE of China, the Korean Research Foundation, GA and MSMT of the Czech Republic, FIAS of Germany, DAE, DST, and CSIR of India, National Science Centre of Poland, National Research Foundation (NRF-2012004024), Ministry of Sci., Ed. and Sports of the Rep. of Croatia, and RosAtom of Russia.

[1] D. de Florian, R. Sassot, M. Stratmann and W. Vogelsang, Phys. Rev. Lett. **101**, 072001 (2008).
[2] D. de Florian, R. Sassot, M. Stratmann and W. Vogelsang, Phys. Rev. D **80**, 034030 (2009).
[3] J. Blumlein and H. Bottcher, Nucl. Phys. B **841**, 205 (2010).
[4] E. Leader, A. V. Sidorov and D. B. Stamenov, Phys. Rev. D **82**, 114018 (2010).
[5] R. D. Ball *et al.* [The NNPDF Collaboration], Nucl. Phys. B **874**, 36 (2013).
[6] C. A. Aidala, S. D. Bass, D. Hasch and G. K. Mallot, Rev. Mod. Phys. **85**, 655 (2013).
[7] L. Adamczyk *et al.* [STAR Collaboration], Phys. Rev. D **86**, 032006 (2012).
[8] B. I. Abelev *et al.* [STAR Collaboration], Phys. Rev. Lett. **100**, 232003 (2008).
[9] B. I. Abelev *et al.* [STAR Collaboration], Phys. Rev. Lett. **97**, 252001 (2006).
[10] S. S. Adler *et al.*, Phys. Rev. D **73**, 091102 (2006).
[11] A. Adare *et al.* [PHENIX Collaboration], Phys. Rev. D **76**, 051106 (2007).
[12] A. Adare *et al.* [PHENIX Collaboration], Phys. Rev. Lett. **103**, 012003 (2009).
[13] A. Adare *et al.* [PHENIX Collaboration], Phys. Rev. D **79**, 012003 (2009).
[14] B. Jäger, M. Stratmann and W. Vogelsang, Phys. Rev. D **70**, 034010 (2004).
[15] Special Issue: RHIC and its Detectors Nucl. Instrum. Meth. A **499**, 624 (2003), and references therein.
[16] O. Jinnouchi *et al.*, arXiv:nucl-ex/0412053.
[17] H. Okada *et al.*, arXiv:hep-ex/0601001.
[18] J. Kiryluk *et al.*. hep-ex/0501072.
[19] G. C. Blazey *et al.*, arXiv:hep-ex/0005012.
[20] M. Cacciari, G. P. Salam and G. Soyez, JHEP **0804**, 063 (2008).
[21] M. Cacciari, G. P. Salam and G. Soyez, Eur. Phys. J. C **72** 1896 (2012).
[22] T. Sjostrand, S. Mrenna and P. Z. Skands, JHEP **0605**, 026 (2006).
[23] Geant 3.21, CERN Program Library.
[24] A. Mukherjee and W. Vogelsang, Phys. Rev. D **86**, 094009 (2012).
[25] R. D. Ball *et al.* [NNPDF Collaboration], Nucl. Phys. B **849**, 112 (2011) [*Errata: ibid* **854**, 926 (2012) and **855**, 927 (2012)].
[26] R. D. Ball, V. Bertone, F. Cerutti, L. Del Debbio, S. Forte, A. Guffanti, N. P. Hartland and J. I. Latorre *et al.*, Nucl. Phys. B **855**, 608 (2012).